A frequent kinase domain mutation that changes the interaction between PI3Kα and the membrane

Diana Mandelker[a,1], Sandra B. Gabelli[b,1,2], Oleg Schmidt-Kittler[a], Jiuxiang Zhu[a], Ian Cheong[a], Chuan-Hsiang Huang[b,3], Kenneth W. Kinzler[a], Bert Vogelstein[a,2], and L. Mario Amzel[b,2]

[a]The Ludwig Center for Cancer Genetics and Therapeutics and Howard Hughes Medical Institute, Johns Hopkins Kimmel Cancer Center, Baltimore, MD 21231; and [b]Department of Biophysics and Biophysical Chemistry, The Johns Hopkins University School of Medicine, Baltimore, MD 21205

Contributed by Bert Vogelstein, August 5, 2009 (sent for review July 13, 2009)

Mutations in oncogenes often promote tumorigenesis by changing the conformation of the encoded proteins, thereby altering enzymatic activity. The *PIK3CA* oncogene, which encodes p110α, the catalytic subunit of phosphatidylinositol 3-kinase alpha (PI3Kα), is one of the two most frequently mutated oncogenes in human cancers. We report the structure of the most common mutant of p110α in complex with two interacting domains of its regulatory partner (p85α), both free and bound to an inhibitor (wortmannin). The N-terminal SH2 (nSH2) domain of p85α is shown to form a scaffold for the entire enzyme complex, strategically positioned to communicate extrinsic signals from phosphopeptides to three distinct regions of p110α. Moreover, we found that Arg-1047 points toward the cell membrane, perpendicular to the orientation of His-1047 in the WT enzyme. Surprisingly, two loops of the kinase domain that contact the cell membrane shift conformation in the oncogenic mutant. Biochemical assays revealed that the enzymatic activity of the p110α His1047Arg mutant is differentially regulated by lipid membrane composition. These structural and biochemical data suggest a previously undescribed mechanism for mutational activation of a kinase that involves perturbation of its interaction with the cellular membrane.

mutant | p110 | p85 | oncogene

The "hotspots" within oncogenes are specific residues that are recurrently mutated in cancers. These mutations result in constitutive protein activation by several mechanisms, including destabilization of an inactive conformation (B-RAF Val600Glu; ref. 1) or locking of the activation loop in an active conformation (K-RAS Gly12Val; ref. 2). These mutated enzymes are especially attractive targets for the rational design of anticancer therapeutics because the mutant enzymes are found exclusively in cancer cells. Successful drug developments based on this principle are exemplified by the EGFR kinase inhibitors gefitinib and erlotinib, both approved for clinical use (3, 4).

PIK3CA was definitively identified as a human oncogene through the discovery of several hotspot mutations in colorectal carcinomas (5). Since then, more than 1,500 *PIK3CA* mutations in diverse tumor types have been discovered (6). The most common mutant is His1047Arg (6), and mutations at this residue in breast and uterine cancers are associated with clinical prognosis (7–9). Biochemical assays have demonstrated that the His1047Arg mutant has a 2-fold increase in lipid kinase activity (10), that its activity increases further upon phosphopeptide binding (10), and that the activity is independent of Ras binding but dependent on p85 binding (11). Despite the frequency and clinical significance of the *PIK3CA* His1047Arg mutation, no unifying mechanism for its oncogenic activation has been reported.

Phosphoinositol 3- kinase alpha (PI3Kα) is a heterodimeric enzyme formed by a catalytic subunit (p110α, encoded by *PIK3CA*) and one of several regulatory subunits (a major one being p85α, encoded by PI3KR1). The p110α subunit contains an N-terminal adaptor-binding domain (ABD) that was proposed to be responsible for binding to p85α, a Ras-binding domain (RBD), a C2 domain that has been proposed to bind to cellular membranes, a helical domain of unknown function, and a catalytic kinase domain (12–14). The p85α subunit contains two SH2 domains that bind phosphorylated tyrosines of receptor tyrosine kinases and adaptor molecules, such as IRS-1. The N-terminal SH2 (nSH2) and an inter-SH2 (iSH2) domain contact the p110α subunit (15). Once activated by binding to the platelet-derived growth factor receptor (PDGFR) or other receptor kinases, the enzyme phosphorylates phosphatidylinositol-4,5-bisphosphate [PI(4,5)P_2, or PIP_2] to generate phosphatidylinositol-3,4,5-triphosphate (PIP_3) at the cell membrane (12, 13). Pleckstrin homology domain-containing proteins, including Akt serine-theronine kinases, bind PIP_3 and are thereby recruited to the cell membrane (16). Proteins such as Akt are then phosphorylated by other membrane-associated enzymes and activate signaling cascades involved in cellular motility, metabolism, proliferation, and survival (17).

The critical role of the PI3K pathway in a variety of disease processes, including neoplasia, has prompted the development of pathway inhibitors. Wortmannin was isolated in 1957 from *Penicillium wortmannii,* (18) and was later shown to be an inhibitor of PI3K enzymes (19). Although wortmannin's instability and toxicity prevent it from being used as a drug in the clinic, a derivative with a more favorable pharmacological profile is currently in clinical trials for the treatment of advanced malignancies (20, 21).

Previous studies have reported the structure of PI3Kγ as both a free enzyme and in complex with inhibitors and the structure of the WT form of PI3Kα. No structure of any naturally occurring mutation of a PI3K enzyme has been reported previously. Here, we report the structure of the most common mutant of PI3Kα, His1047Arg, alone and in complex with wortmannin.

Results

Crystallization. We have shown previously that the WT PI3Kα enzyme can be expressed in a form suitable for structural studies in a complex containing the entire catalytic subunit and the nSH2 and iSH2 domains (hereafter termed "niSH2") of the p85α subunit. When expressed in Sf9 cells through a baculovirus vector under the same conditions, no significant yield of the His1047Arg mutant

Author contributions: S.B.G., K.W.K., B.V., and L.M.A. designed research; D.M., O.S.-K., J.Z., I.C., and C.-H.H. performed research; J.Z. contributed new reagents/analytic tools; D.M., S.B.G., O.S.-K., K.W.K., B.V., and L.M.A. analyzed data; and D.M., S.B.G., B.V., and L.M.A. wrote the paper.

Conflict of interest statement: The authors declare a conflict of interest (such as defined by PNAS policy). Under agreements between The Johns Hopkins University and various commercial entities, K.W.K. and B.V. are entitled to a share of the royalties received by The Johns Hopkins University on sales of products related to the diagnosis of mutant PIK3CA genes. The terms of these arrangements are being managed by The Johns Hopkins University in accordance with its conflict of interest policies.

Data deposition: The atomic coordinates of the p110α His1047Arg/niSH2 enzyme, both free and in complex with wortmannin, have been deposited in the Protein Data Bank (PDB ID codes 3HIZ and 3HHM).

[1]D.M. and S.B.G. contributed equally to this work.

[2]To whom correspondence may be addressed. E-mail: gabelli@jhmi.edu, vogelbe@jhmi.edu, and mamzel@jhmi.edu.

[3]Present address: Department of Cell Biology, The Johns Hopkins University, Baltimore, MD 21205.

This article contains supporting information online at www.pnas.org/cgi/content/full/0908444106/DCSupplemental.

Table 1. Data collection and refinement statistics

	Crystal	
	p110α His1047Arg/ niSH2 plus wortmannin	p110α His1047Arg/niSH2
Space group	$P2_12_12_1$	
Cell dimensions		
a, Å	115.3	115.3
b, Å	119.4	120.6
c, Å	152.5	153.9
α, °	90	90
β, °	90	90
γ, °	90	90
Data collection statistics		
X-ray source	APS	APS
Wavelength, Å	0.97929	0.97929
Resolution, Å	50–2.8 (2.9–2.8)	50–3.3 (3.42–3.3)
Measured reflections	362,120	221,197
Unique reflections	53,371	32,487
I/σ	23.6 (2.0)	17.9 (2.47)
Completeness, %	99.8 (99.6)	99.5 (98.3)
R_{merge}, %	9.3 (68.9)	8.6 (48.1)
Refinement		
R_{cryst}, %	24.4	26.3
R_{free}, %	30.9	33.2
rmsd		
Bond length, Å	0.008	0.011
Angle, °	1.302	1.431
Monomers in asymmetric unit	1	1
Total atoms	10,727	10,383
Protein atoms	10,581	10,383
Water molecules	115	0
Ligand	1	0
B factor (protein), Å^2	75.87	86.0
B factor (ligand), Å^2	62.24	N/A
B factor (H_2O), Å^2	61.75	N/A

N/A indicates not applicable.

protein of p110α could be obtained. We therefore infected these cells with baculoviruses in the presence of a specific inhibitor of PI3Kα called J32 (Fig. S1 and Scheme in *SI Appendix*). Similar uses of inhibitors to increase the yield of toxic, exogenous kinases have been described previously (22). We found that in the presence of J32, the His1047Arg mutant p110α bound to the niSH2 domains of p85α could be obtained in sufficient yield for crystallization. Diffraction data to resolutions of 2.8 and 3.3 Å were obtained from crystals with and without wortmannin, respectively, and were refined to R_{cryst}/R_{free} values of 24.4/30.9 and 26.3/33.2, respectively (Table 1). Both structures maintained the overall triangular shape observed in the WT structure (23) (Fig. 1*A*).

The nSH2 Domain of p85α Forms a Scaffold for the Enzyme. Although the diffraction data of the WT p110α–niSH2 complex yielded only weak electron density for the nSH2 domain of p85α, the His1047Arg mutant form of the complex revealed a well-ordered nSH2. Although the reasons for this difference are not clear, it provided an opportunity to directly assess the structure of the nSH2–p110α interface. There have been no previous studies of this interface because p110γ, unlike p110α, is stable in the absence of a regulatory subunit and has not been crystallized in a heterodimeric complex. Overall, the p85α nSH2 domain (residues 326–363 and 366–432) in complex with p110α His1047Arg has the same α plus β-fold identified in the crystal structure of the isolated p85α nSH2 domain (24). The structure determined in this work shows that nSH2 acts as a broad-based scaffold for the p110α catalytic subunit, interacting with three of its five domains (the C2, helical, and kinase domains) as well as the p85α iSH2 domain (Figs. 1*B* and 2*A*). From this strategic position, nSH2 is poised to coordinate communication between its four interacting partners: any change in one domain in response to an external stimulus may be sensed by nSH2 and relayed to the others.

Interactions of nSH2 with C2, Helical, and Kinase Domains. The αA helix of nSH2 (residues 340–345) fits into a cavity lined on one side by the C2 domain and the other side by the kinase domain (Fig. 2*B*). The nSH2–kinase interaction is mediated by kinase helix α11K (residues 1017–1024, kα10 in pi3kγ), which is in proximity to helix αA of nSH2. nSH2 and C2 interact through charge interactions, with C2 negatively charged and nSH2 positively charged (Fig. 2*C*). Specific interactions involve nSH2 loops (residues 374–377 and 350–354) interacting with C2 residues 364–371. A salt bridge is observed between nSH2 residue Glu-349 and C2 residue Arg-357. Additionally, nSH2 residue Glu-348 makes two H bonds to C2 residues Glu-453 and Asp-454 (Fig. 2*C*). A mutation observed in glioblastoma in the nSH2 domain, Gly376Arg, is part of this interface (25, 26). The carbonyl of Gly-376 is at hydrogen-bonding distance of Glu-365 of the C2 domain, both in complementary shaped loops.

The interface between nSH2 and the helical domain is dominated by charge interactions: the helical domain is predominately negatively charged, and the nSH2 domain is positively charged. The two hotspot mutations in the helical domain, at residues 542 and 545, directly interact with residues in nSH2. Glu-542 forms a salt bridge with Arg-358 of nSH2, and Glu-545 is parallel to the nSH2 Lys-379 (Fig. 2*D* and Fig. S2).

The structure of a complex between the p85α nSH2 domain and a peptide from PDGFR containing a phosphorylated tyrosine residue has been described previously (24). A comparison of this structure with that of the p110α–p85 niSH2 heterodimeric complex reported here reveals a striking colocalization: the loop of the helical domain (residues 542–546) that contains the hotspot mutations is located precisely where the phosphopeptide binds to nSH2

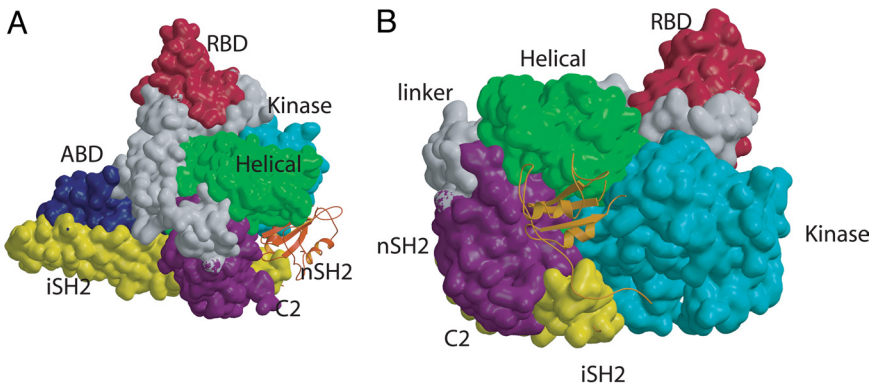

Fig. 1. Overall structure of the complex between the His1047Arg mutant of p110α and the niSH2 domain of p85α. (*A*) Space-filling model of mutant p110α and p85α iSH2 plus ribbon diagram of p85α nSH2. (*B*) Rotated view of His1047Arg mutant p110α and p85α niSH2. nSH2 is shown in ribbon format, contacting the kinase, helical, and C2 domains of p110α and p85α iSH2. Colors used in this and all other figures, except where indicated otherwise, are: in p85α, the iSH2 domain is yellow, and the nSH2 domain is orange; in p110α, the kinase domain is light blue, the helical domain is green, the C2 domain is purple, the RBD is red, and the ABD is dark blue.

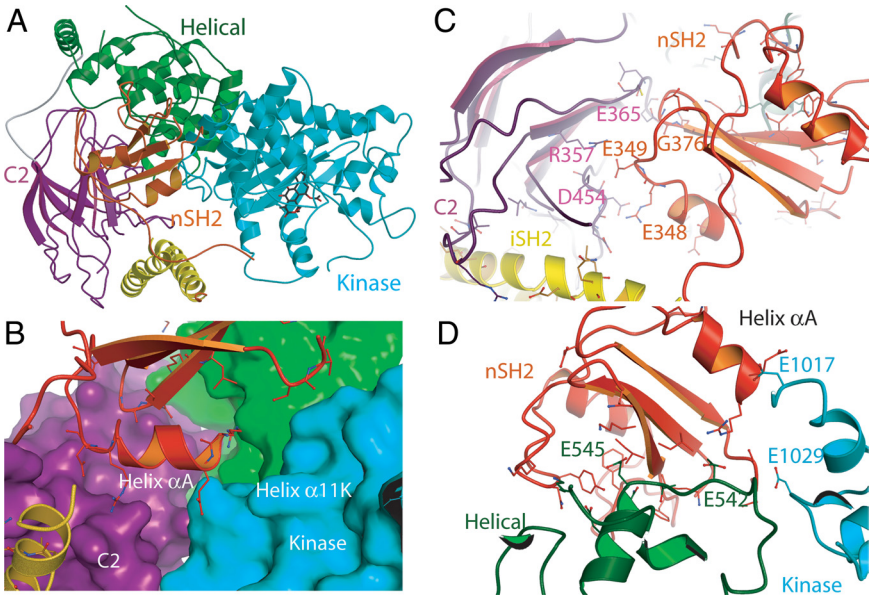

Fig. 2. The nSH2 domain of p85α forms a scaffold for the PI3Kα enzyme. (*A*) p85α nSH2 acts as a scaffold and interacts with the p85α iSH2 domain as well as the p110α kinase, helical, and C2 domains. (*B*) The nSH2 αA helix fits into a crevice between the C2 and kinase domains. (*C*) nSH2 interactions with the p110α C2 domain. (*D*) Residue-residue interactions between nSH2 and the helical and kinase domains.

(Fig. 3 *A* and *B*). Moreover, the side chain of Glu-542 occupies the space usually occupied by the phosphate of the phosphotyrosine in the peptide (Fig. 3*C*). Therefore, phosphopeptides that release the nSH2-mediated inhibition of p110α must shift the orientation of nSH2 relative to the helical domain because both the peptide and helical domain cannot concurrently occupy the same space. The hotspot mutations in the helical domain will have the same effect as binding of physiological phosphopeptides: they interfere with nSH2 binding to p110α, releasing the inhibition. These structural data therefore explain prior biochemical observations demonstrating that the hotspot mutations within the helical domain release the inhibitory effect of nSH2 on the enzyme's activity (27). These observations also support the hypothesis that the His1047Arg structure described here corresponds to an nSH2-inhibited conformation.

Effect of Wortmannin Binding to the Kinase Domain. Wortmannin binds the p110α kinase domain at the ATP-binding site and packs between p110α residues Ile-800, Ile-848, Val-850, and Val-851 on one side, and residues Ser-919, Met-922, Phe-930, Ile-932, and Asp-933 on the other. These residues are equivalent to p110γ residues Ile-831, Ile-879, Ile-881, and Val-882 and residues Asp-950, Met-953, Phe-961, Ile-963, and Asp-964, respectively. This pocket is conserved between p110α and p110γ, with the exception of Ser-919 in p110α, which is Asp-950 in p110γ. Wortmannin forms a covalent bond to the primary amine of Lys-802 (equivalent to Lys-833 is p110γ) and forms four H bonds to active site residues. The O3 atom of wortmannin makes two H bonds to the amide bond of Asp-933 and to the hydroxyl group of Tyr-836; O4 forms an H bond to the amide of Val-851, and O7 forms an H-bond to the side-chain NH of Gln-859 (Fig. 4*A*).

A notable feature of the structure of this complex is a conformational shift of a loop in p110α upon binding to wortmannin: the main chain of the kinase domain loop formed by residues 772–777 moves 3 Å from the position it has in either the Arg-1047 mutant or WT p110α structures in the absence of drug (Fig. 4 *B* and *C*). This shift away from the position occupied by wortmannin in the inhibited complex must reflect changes caused by wortmannin binding. No shift has been reported in the equivalent loop (residues 804–809) of p110γ (Fig. 4*D*) (28). The loops containing residues 197–204 and 228–239 within the RBD are also shifted in the wortmannin-containing structure because the shift of loop 772–777 affects a crystal contact between the RBD and the kinase domain (Fig. S3). In p110γ, three loops (residues 748–750, 832–838, and 871–876) experience conformational changes upon binding wortmannin (28). The equivalent residues in p110α correspond to residues 718–720, 801–807, and 840–845. The latter two of these loops have the same conformation in the p110γ structure with wortmannin, the WT p110α without wortmannin, and the p110α His1047Arg mutant with and without wortmannin structures. Loop 718–720 is a perfect α-helix in both the uninhibited and inhibited p110α structures, whereas it loses its helical conformation in the p110γ structure upon wortmannin binding. Thus, binding of wortmannin elicits different conformations in the two PI3K isoforms that could, in principle, be exploited for the design of isoform-specific inhibitors.

Structural Effects of the His1047Arg Mutation. The histidine normally present at residue 1047 is within H-bonding distance of the main-chain carbonyl of Leu-956, a residue within the activation loop (23). The mutant arginine side chain of 1047 points 90° away from the position of its WT counterpart histidine and greatly increases the distance between it and Leu-956. As a result, the mutant arginine is not likely to fix the activation loop through interaction with Leu-956. On the other hand, this change in orientation causes Arg-1047 to reside in a crevice in the kinase domain, pointing upward toward the modeled cell membrane (Fig. 5*A*). Moreover, the higher pK_a of arginine makes it more likely to interact with negatively charged phospholipid head groups than with histidine. The Arg-1047 mutation has an additional effect: it orders 13 residues of p110α near the C terminus. Residues 1050–1062, which were disordered in the WT structure, folded in the mutant as a loop positioned to interact with the cell membrane (Fig. 5*B*). Moreover, another loop of the kinase domain, previously proposed to interact with the cell membrane (residues 864–874), has a different conformation in the His1047Arg mutant than in the WT enzyme (Fig. 5*C*). This change in conformation is required because the WT orientation of this loop would clash with the position of the 1050–1062 loop in the mutant. Taken together, these structural changes suggest that the His1047Arg mutation may act by altering the interaction of p110α with the cell membrane, an interaction vital to the enzyme's lipid kinase activity (Fig. 5*A*).

Curiously, the WT p110γ protein contains an arginine at residue 1076 (corresponding to residue 1047 in p110α). This has suggested that p110γ can be regarded as a naturally occurring His1047Arg mutant (29). However, the structures presented here show that

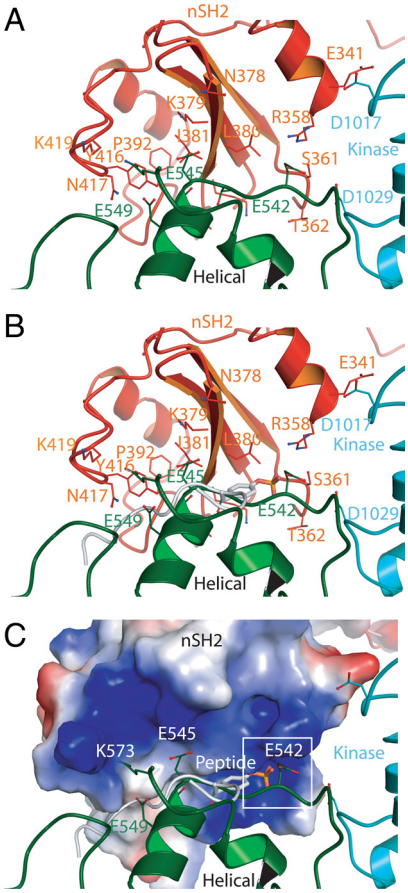

Fig. 3. Interactions between p110α and p85 nSH2. (*A*) Ribbon diagram of nSH2, helical, and kinase domains determined from the structure reported in this work. (*B*) The same ribbon diagram as in *A* but showing the position of the PDGFR phosphopeptide (gray) modeled as in PDB ID code 2IUI, at the interface between nSH2 and the helical domain. The loop of the helical domain occupies nearly the same position as the phosphopeptide, so their occurrence is mutually exclusive. (*C*) The phosphopeptide is predicted to disrupt the interaction between the positively charged nSH2 surface (shaded blue) and the negatively charged helical domain residues. The phosphopeptide is shown in gray, with its phosphotyrosine in stick and ball representation and the phosphate shaded red. The boxed region shows that the side chain of Glu-542 occupies the space usually occupied by the phosphate of the peptide's phosphotyrosine residue.

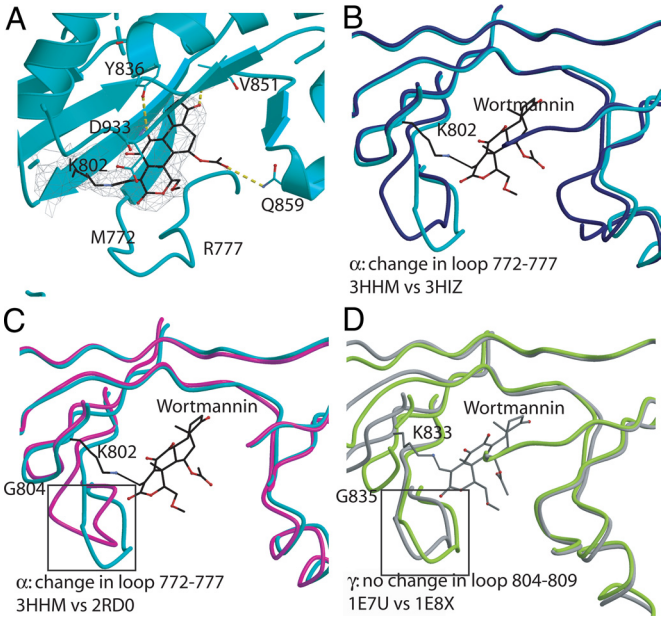

Fig. 4. Wortmannin and its effect on the kinase domain ATP-binding site. (*A*) Wortmannin makes four H bonds to kinase domain residues and covalently attaches to Lys-802. Electron density for the wortmannin ligand is shown. (*B*) Upon binding PI3Kα His1047Arg (PDB ID code 3HHM), wortmannin induces a shift of loop 772–777 (light blue) compared with the same mutant enzyme in the absence of wortmannin (PDB ID code 3HIZ; navy blue). (*C*) Loop 772–777 is shifted for PI3Kα His1047Arg (PDB ID code 3HHM; light blue), compared with WT PI3Kα (PDB ID code 2RD0; pink). (*D*) In PI3Kγ, wortmannin binding has no effect on the conformation of loop 804–809, the residues equivalent to 772–779 in PI3Kα.

there are major differences between the catalytic domains of the His1047Arg mutant of p110α and the WT p110γ. Although the main chains of these two proteins are in close proximity, the two equivalent arginine residues point 180° from each other. Moreover, in p110γ, Arg-1076 occurs in a helix, whereas in p110α, Arg-1047 is located in a loop. Therefore, the structure of the kinase domain of the Arg-1047 mutant represents a unique oncogenic conformation, distinct from the WT p110α and from p110γ.

Enzymatic Activity Depends on Membrane Composition. The structural differences described above suggest that the activation of the His1047Arg mutant takes place through a change in the way p110α interacts with the cell membrane. Experiments were devised to test this hypothesis by studying the effect of membrane composition on the activity of p110α. The lipid kinase activities of WT and His1047Arg mutant forms of p110α were measured in the presence of five different lipids: 1,2-diacyl-*sn*-glycero-3-phospho-L-serine (PS), lipids extracted from the cancer cell lines DLD1 and HCT116, and lipids extracted from brain and liver tissues. Under the assay conditions used, the lipids form bilayered membranous vesicles containing the added PIP_2 substrate (30). The enzyme binds to these vesicles and phosphorylates the PIP_2 substrate at the outer leaflet of the bilayer. The relative activities of the WT and mutant forms were found to be differentially regulated by lipid composition (Fig. 5*D*). For example, with lipids from HCT116 and DLD1 cells, the mutant's enzymatic activity increased approximately twice as much as that of WT (2.5-fold vs. 1.2-fold) with respect to their activities in PS-containing vesicles. For the His1047Arg mutant, the enzymatic activity in conditions containing liver lipid extract was the same as its activity in the presence of PS. Conversely, the WT enzyme's activity in the liver lipid conditions decreased by nearly 50%. Control experiments showed that these differences did not depend on different amounts of endogenous substrate in the various lipid preparations, because there was relatively little activity in the absence of added PIP_2 in any of the five lipid preparations. One potential explanation for these observations is that the different lipids exerted their effects by changing the size of the vesicles, and therefore their curvature. However, we found no correlation between the size of the vesicles and the relative activities of the enzymes (Fig. S4), indicating that the differential activities of the mutant and WT proteins reflect the different lipid compositions of the vesicles. The activity measurements provide strong support for the hypothesis, based on the new structure, that the His1047Arg mutation alters the interaction of the kinase domain with the cell membrane. In turn, the accessibility of the substrate to the binding site of the enzyme would be enhanced, increasing its activity.

Discussion

Oncogenic mutations in the catalytic domains of kinases are generally thought to increase activity by affecting activation-loop conformations. However, for the His1047Arg mutant of p110α, the mutation in the kinase domain has no apparent effect on the structure of the catalytic sites. The p110α activation loop had no electron density in the WT PI3Kα structure (23), suggesting that these residues were mobile. Surprisingly, there was also no electron

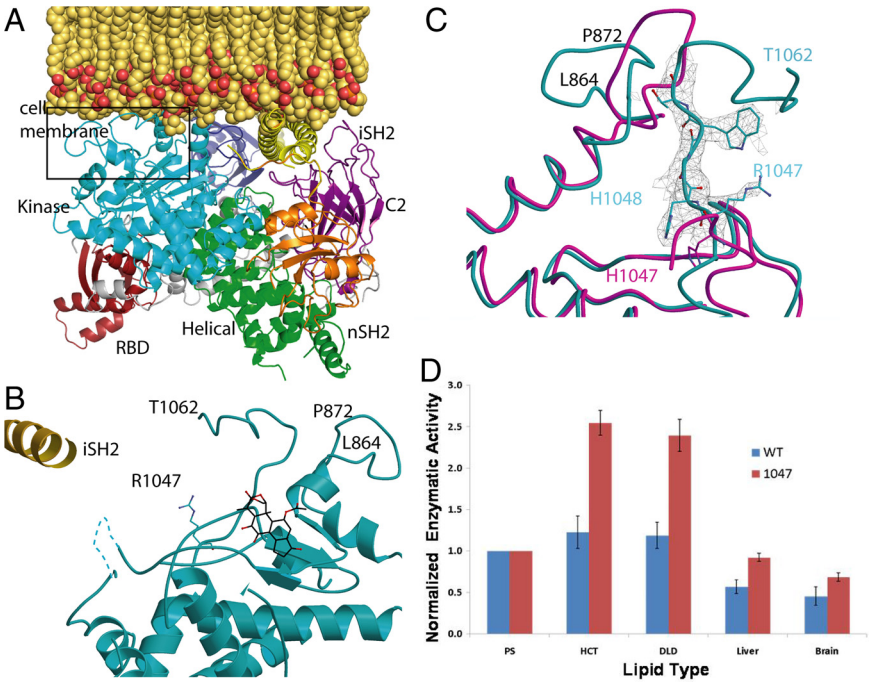

Fig. 5. Effects of the His1047Arg mutation on the structure of the enzyme. (*A*) Ribbon diagram showing the mutant enzyme's position relative to the modeled cell membrane. The two loops of the kinase domain that are predicted to contact the membrane are boxed. (*B*) Two loops (residues 864–874 and 1050–1062) change conformation and contact the cell membrane. Arg-1047 changes its orientation by 90° and points upward to the membrane. (*C*) Differences in conformation of loops 864–874 and 1050–1064 between WT (pink) and His1047Arg (light blue) structures. The electron density corresponding to residues 1047–1052 of the mutant structure is highlighted. (*D*) The enzymatic activity of WT and His1047Arg mutants of p110α was differentially regulated by membrane lipid composition. The activities of the WT and mutant enzymes were normalized to the activity measured with PS lipids; the unnormalized activity of the mutant with PS vesicles was 2.1-fold higher than that of the WT. The experiment was performed three times, with duplicate determinations for each experiment. The means (bars) and SDs (brackets) of one representative experiment are shown.

density for these residues in the His1047Arg mutant structure, making it unlikely that the His1047Arg mutation locks the activation loop in a fixed conformation. Conversely, the striking effect of this mutation on the orientation of the 1047 residue and on two loops that contact the cell membrane strongly suggests a previously undescribed mechanism of action for an oncogenic mutation in a catalytic domain. Biochemical assays show a remarkable effect of lipid membrane composition on the activity of the His1047Arg mutant compared with the WT form of the enzyme. Only changes in the proteins' relative abilities to interact with membranes could account for this differential effect of lipids on enzymatic activity, because all other components of these biochemical assays were identical. Therefore, the His1047Arg mutation likely causes increased lipid kinase activity by allowing easier access to the membrane-bound PIP_2 substrate, which is then converted to PIP_3, initiating tumorigenic signaling cascades.

This mechanism may explain several previously puzzling observations on the His1047Arg mutant of *PIK3CA*. Zhao and Vogt (11) demonstrated that the activation of this mutant is independent of Ras binding. Ras is attached to the cell membrane through a farnesyl group and binds the Ras-binding domain of p110α through the RBD. Therefore, Ras may function to activate the WT form of p110α by increasing tethering of p110α to the cell membrane, where it can access its PIP_2 substrate. The His1047Arg mutation may circumvent the need for Ras binding by independently localizing p110α to the membrane through conformational shifts in the kinase domain loops 864–874 and 1050–1062. Further support for the importance of membrane binding on the activity of PI3Kα is provided by genetically engineered forms of p110α. When a myristylation site is engineered into p110α, its resultant constitutive membrane binding activates Akt and other downstream targets in a pattern identical to that of the His1047Arg mutant (31–33). Similarly, fusion proteins in which WT p110α is joined to retroviral Gag sequences render the enzyme constitutively active by virtue of the membrane address supplied by the Gag domain (31, 32). Finally, the oncogenic transforming activity of the myristylated or Gag-fusion forms of p110α is identical to that of the naturally occurring His1047Arg mutant in the absence of membrane tags (31–33).

The His1047Arg mutation has been identified in cancers of the breast, colon, uterus, stomach, ovary, and numerous other organs. In addition to the effects of this mutation on membrane interactions, the conformational shift upon wortmannin binding is considerably different from that observed with p110γ. These results should facilitate the development of a new generation of isoform- and mutant-specific PI3Kα inhibitors that exploit the altered ATP-binding site conformation as well as the previously undescribed membrane–protein interactions.

Methods

Cloning of Mutant and WT Forms of p110α. The human His1047Arg mutant transcript was amplified by reverse-transcriptase-coupled PCR using mRNA from the colorectal cancer cell line HCT116 (forward primer, 5′-tattggatccatgcctccaagaccatc-3′; reverse primer, 5′-gtacaagcttcagttcaatgcatgctg-3′) and was cloned with BamHI and HindIII into pFastBac-HT-A (Invitrogen). The WT form of the transcript was amplified from a clone obtained from Genecopoeia. Baculovirus clones of these constructs were generated by using the Invitrogen Bac-to-Bac Baculovirus Expression System (Invitrogen). The cloning of niSH2 has been described previously (23).

Protein Expression. Sf9 cells were grown in suspension culture in Sf-900 III Serum Free Media (Invitrogen) supplemented with 0.5% penicillin-streptomycin at room temperature. At a density of 4×10^6 cells per milliliter, cells were infected with p110α His1047Arg and p85α niSH2 viruses at a multiplicity of infection ratio of 3:2. A total of 60 nM PI3K inhibitor J32 (see Scheme in *SI Appendix*) was added to the media at the time of infection. The addition of inhibitor increased the protein yield from an undetectable amount on a Coomasie brilliant blue-stained gel to 1 mg per 1.2×10^{10} cells. At 72 h after infection, cells were harvested by centrifugation at 900 $\times$ *g*. The protein purification scheme has been described previously (23).

Crystallization. For cocrystallization with wortmannin, purified protein at 15 mg/mL was mixed with the drug to a final drug concentration of 100 μM. Screening was conducted in hanging drops at 20 °C around the crystallization conditions of the WT form of the PI3Kα complex (1.4 M sodium formate and 100 mM Hepes, pH 7.0) (23). We identified crystals in one condition (0.8 M sodium formate and 100 mM Hepes, pH 6.8), and a silver bullet (HR2-096; Hampton Research) additive screen was then performed. Larger crystals were obtained in the well containing the additive mixture: 0.2% (wt/vol) rhenium (IV) oxide, 0.2% (wt/vol) sodium bromide, 0.2% (wt/vol) sodium nitrate, 0.2% (wt/vol) sodium dibasic phosphate dihydrate, 0.2% (wt/vol) sodium tetraborate decahydrate, and 0.02 M Hepes, pH 6.8. Diffracting crystals (0.4 $\times$ 0.08 mm in size) were obtained by iterative rounds of macroseedings in 0.65 M sodium formate; 100 mM Hepes, pH 6.8; and 25% silver bullet. The conditions for crystallization in the absence of

wortmannin required a higher concentration of sodium formate (1.2 M sodium formate and 100 mM Hepes, pH 6.8). Crystals were flash frozen in liquid nitrogen by using the reservoir solution plus 10% glycerol as cryoprotectant.

Data Collection. X-ray diffraction data were collected at the Lily Research Laboratory Collaborative Access Team (LRL-CAT) beamline at section 31 of the Advanced Photon Source and were processed with HKL2000 (Table 1). The crystals diffracted to a resolution of 2.8 Å in the presence of wortmannin and 3.3 Å in the absence of wortmannin.

Structure Determination. The structure of the wortmannin complex was determined by using the coordinates of WT p110α/NiSH2 [Protein Data Bank (PDB) ID code 2RD0] as a model. After rigid body and positional refinement, the program O (34) was used for model building. The initial round of refinement showed that the nSH2 domain of p85α was present and ordered in the structure. Therefore, the p85α nSH2 crystal structure (PDB ID code 2IUG) (24) was used as a guide to fit the additional electron density in this region. Iterative rounds of refinement using REFMAC 5.0 (35) yielded a final R of 24.4% and an R_{free} of 30.9% to 2.8 Å in the presence of wortmannin. The protein coordinates of this structure were used as the initial model for the determination of the structure in the absence of wortmannin; refinement yielded an R_{cryst} of 26.3% and an R_{free} of 33.2% to 3.3 Å (Table 1).

Lipid Extraction. Methods for lipid extraction were adapted from Folch's procedure (36). Briefly, HCT116 and DLD1 cells were harvested by using trypsin/EDTA. The cells were pelleted, washed with PBS, and resuspended in 20 volumes of chloroform–methanol [2:1 (vol/vol)]. These suspensions were vortexed for 1 min and mixed on a Labquake Rotator (Barnstead/Thermolyne model 415110) for 20 min at room temperature. Next, the suspensions were centrifuged at 5,000 $\times$ g for 10 min and decanted through filter paper. A total of 0.2 volumes of 0.9% NaCl solution was added to each filtrate and vortexed for 30 seconds. After centrifugation at 5,000 $\times$ g for 10 min, the upper phase was aspirated and discarded. Next, the interface was gently washed once with methanol–water [1:1 (vol/vol)]. The remaining lower phase was transferred to a glass vial and dried by using a BÜCHI Rotavapor R-200 (BÜCHI Labortechnik). The dried samples were used for liposome preparation. The sizes of the liposomes were determined by quasielastic light scattering using a Malvern Zetasizer Nano S (Malvern). Briefly, liposomes suspended in PBS were dispensed into cuvettes and illuminated with a laser. The fluctuations in intensity of the scattered laser light were then measured by the Zetasizer. Because the rate of fluctuations is directly related to the Brownian motion of the liposomes, and hence their hydrodynamic radii, the liposomal size distribution may be calculated by using the Stokes–Einstein equation.

p110α/niSH2 Enzyme Kinetics. The protein concentrations of the purified proteins were determined with a Bradford assay (BioRad) and adjusted to 1.8 mg/mL with 10 mM Tris·HCl (pH 8.5), 25 mM NaCl, 1 mM DTT, and 50% glycerol. Enzyme activities were determined in the presence of 0.05 mg/mL lipids derived from purified PS (Sigma), extracts of liver (Avanti Polar Lipids) and brain (Avanti Polar Lipids), or HCT116 and DLD1 cell lines. In addition, the reaction mix contained 0.05 μg/μL L-a-phosphatidylinositol-4,5-bisphosphate (Avanti Polar Lipids); 100 μM ATP; 40 μCi/mL γ-[^{32}]ATP (Perkin–Elmer); 2.5 mM $MgCl_2$; 5 mM Hepes, pH 7.5; and 6 ng/mL purified p110α. At various times, aliquots of the master reaction were taken, the reaction stopped with 1 volume of 2 M HCl, and the lipids extracted with 2 volumes of chloroform–methanol (1:1). A total of 10 μL of the organic phase was mixed with 80 μL of microscint O scintillation fluid (Perkin–Elmer), and the incorporated radioactivity was measured with a TopCount 96-well plate scintillation counter (Perkin–Elmer).

ACKNOWLEDGMENTS. We thank Dr. George Sgouros and Dr. Yah-el Har-el for use of the Zetasizer. Use of the APS at Argonne National Laboratory was supported by the U.S. Department of Energy, Office of Science, Office of Basic Energy Sciences, under Contract No. DE-AC01-06CH11357. Use of the LRL-CAT beamline at Sector 31 of the APS was provided by Eli Lilly & Company, which operates the facility. Support was provided by the Virginia and D.K. Ludwig Fund for Cancer Research and National Institutes of Health Grants CA43460, GM07309, and GM07184.

1. Wan P, et al. (2004) Mechanism of activation of the RAF-ERK signaling pathway by oncogenic mutations of B-RAF. *Cell* 116:855–867.
2. Al-Mulla F, Milner-White E, Going J, Birnie GD (1999) Structural differences between valine-12 and aspartate-12 Ras proteins may modify carcinoma aggression. *J Pathol* 187:433–438.
3. Fukuoka M, et al. (2003) Multi-institutional randomized phase II trial of gefitinib for previously treated patients with advanced non-small-cell lung cancer (The IDEAL 1 Trial). *J Clin Oncol* 21:2237–2246.
4. Shepherd F, et al. (2005) Erlotinib in previously treated non-small-cell lung cancer. *N Engl J Med* 353:123–132.
5. Samuels Y, et al. (2004) High frequency of mutations of the PIK3CA gene in human cancers. *Science* 304:554.
6. Database of clinical trials. Available at: http://www.sanger.ac.uk/genetics/CGP/cosmic/. Accessed May 10, 2009.
7. Lai Y, et al. (2008) PIK3CA exon 20 mutation is independently associated with a poor prognosis in breast cancer patients. *Ann Surg Oncol* 15:1064–1069.
8. Lerma E, et al. (2008) Exon 20 PIK3CA mutations decreases survival in aggressive (HER-2 positive) breast carcinomas. *Virchows Arch* 453:133–139.
9. Catasus L, Gallardo A, Cuatrecasas M, Prat J (2008) PIK3CA mutations in the kinase domain (exon 20) of uterine endometrial adenocarcinomas are associated with adverse prognostic parameters. *Mod Pathol* 21:131–139.
10. Carson JD, et al. (2008) Effects of oncogenic p110alpha subunit mutations on the lipid kinase activity of phosphoinositide 3-kinase. *Biochem J* 409:519–524.
11. Zhao L, Vogt PK (2008) Helical domain and kinase domain mutations in p110alpha of phosphatidylinositol 3-kinase induce gain of function by different mechanisms. *Proc Natl Acad Sci USA* 105:2652–2657.
12. Cantley LC (2002) The phosphoinositide 3-kinase pathway. *Science* 296:1655–1657.
13. Vanhaesebroeck B, Waterfield MD (1999) Signaling by distinct classes of phosphoinositide 3-kinases. *Exp Cell Res* 253:239–254.
14. Vivanco I, Sawyers CL (2002) The phosphatidylinositol 3-kinase AKT pathway in human cancer. *Nat Rev Cancer* 2:489–501.
15. Yu J, Wjasow C, Backer JM (1998) Regulation of the p85/p110alpha phosphatidylinositol 3′-kinase. Distinct roles for the n-terminal and c-terminal SH2 domains. *J Biol Chem* 273:30199–30203.
16. Vanhaesebroeck B, Alessi DR (2000) The PI3K-PDK1 connection: More than just a road to PKB. *Biochem J* 346:561–576.
17. Katso R, et al. (2001) Cellular function of phosphoinositide 3-kinases: Implications for development, homeostasis, and cancer. *Annu Rev Cell Dev Biol* 17:615–675.
18. Brian PW, Curtis PJ, Hemming HG, Norris GLF (1957) Wortmannin, an antibiotic produced by Penicillium wortmanni. *Trans Br Mycol Soc* 40:365–368.
19. Arcaro A, Wymann M (1993) Wortmannin is a potent phosphatidylinositol 3-kinase inhibitor: The role of phosphatidylinositol 3,4,5-trisphosphate in neutrophil responses. *Biochem J* 296:297–301.
20. Ihle N, et al. (2004) Molecular pharmacology and antitumor activity of PX-866, a novel inhibitor of phosphoinositide-3-kinase signaling. *Mol Cancer Ther* 3:763–772.
21. Database of clinical trials. Available at: http://clinicaltrials.gov/ct2/show/NCT00726583. Accessed May 10, 2009.
22. Strauss A, et al. (2007) Improved expression of kinases in Baculovirus-infected insect cells upon addition of specific kinase inhibitors to the culture helpful for structural studies. *Protein Expr Purif* 56:167–176.
23. Huang CH, et al. (2007) The structure of a human p110alpha/p85alpha complex elucidates the effects of oncogenic PI3Kalpha mutations. *Science* 318:1744–1748.
24. Nolte R, Eck M, Schlessinger J, Shoelson S, Harrison S (1996) Crystal structure of the PI 3-kinase p85 amino-terminal SH2 domain and its phosphopeptide complexes. *Nat Struct Biol* 3:364–374.
25. Parsons DW, et al. (2008) An integrated genomic analysis of human glioblastoma multiforme. *Science* 321:1807–1812.
26. Cancer Genome Atlas Research Network (2008) Comprehensive genomic characterization defines human glioblastoma genes and core pathways. *Nature* 455:1061–1068.
27. Miled N, et al. (2007) Mechanism of two classes of cancer mutations in the phosphoinositide 3-kinase catalytic subunit. *Science* 317:239–242.
28. Walker EH, et al. (2000) Structural determinants of phosphoinositide 3-kinase inhibition by wortmannin, LY294002, quercetin, myricetin, and staurosporine. *Mol Cell* 6:909–919.
29. Amzel LM, et al. (2008) Structural comparisons of class I phosphoinositide 3-kinases. *Nat Rev Cancer* 8:665–669.
30. Barnett S, et al. (1995) Interfacial catalysis by phosphoinositide 3′-hydroxykinase. *Biochemistry* 34:14254–14262.
31. Aoki M, et al. (2000) The catalytic subunit of phosphoinositide 3-kinase: Requirements for oncogenicity. *J Biol Chem* 275:6267–6275.
32. Denley A, Kang S, Karst U, Vogt PK (2008) Oncogenic signaling of class I PI3K isoforms. *Oncogene* 27:2561–2574.
33. Kang S, Denley A, Vanhaesebroeck B, Vogt PK (2006) Oncogenic transformation induced by the p110beta, -gamma, and -delta isoforms of class I phosphoinositide 3-kinase. *Proc Natl Acad Sci USA* 103:1289–1294.
34. Jones T, Kjeldgaard M (1997) Electron-density map interpretation. *Methods Enzymol* 277:173–208.
35. Collaborative Computational Project, Number 4 (1994) The CCP4 suite: Programs for protein crystallography. *Acta Crystallogr D Biol Crystallogr* 50:760–763.
36. Folch J, Lees M, Sloane Stanley GH (1957) A simple method for the isolation and purification of total lipides from animal tissues. *J Biol Chem* 226:497–509.